A PMSM Model Incorporating Structural and Saturation Saliencies

Ying Yan[1], Jianguo Zhu[1], Haiwei Lu[1], Youguang Guo[1] and Shuhong Wang[2]
[1]Faculty of Engineering, University of Technology, Sydney, PO Box 123, Broadway, NSW 2007, Australia
[2]Faculty of Electrical Engineering, Xi'an Jiaotong University, Xi'an, 710049, China

Abstract—**Sensorless permanent magnet synchronous motor (PMSM) drive systems have become very attractive due to their advantages, such as the reduction of hardware complexity and hence the reduced system cost and increased reliability. In order to accurately determine the rotor position required for correct electronic commutation, various methods have been proposed. Among them, the most versatile makes use of the structural and/or magnetic saturation saliencies of the PMSM. This paper presents a non-linear model for PMSMs with the saliencies. The phase inductances of a PMSM are measured and expressed by Fourier series at different rotor positions according to their patterns. The dynamic performance of the PMSM is simulated and compared with that based on a model without considering saliency to verify the effectiveness of the proposed model.**

I. Introduction

Sensorless control of permanent magnet synchronous motors (PMSMs) has become very attractive because of its many advantages over the systems with mechanical position and/or speed sensors, such as significant reduction of system hardware complexity and increase of the system reliability. A great amount of research has been conducted on position sensorless techniques and various methods have been proposed. Among them, the most versatile is to detect the structural and/or magnetic saturation saliencies of the PMSM [1-2].

Generally, there are two types of saliencies within an electric machine: structural saliency and magnetic saturation saliency. The structural saliency is caused by the mechanical structure of the machine. For the electric machines with large structural saliency, e.g. interior type PMSM, the structural saliency-based rotor position identification can be very effective.

The magnetic saturation saliency is caused by the saturation of magnetic core. In a PMSM, this kind of saliency is mainly caused by the permanent magnets (PMs) on the rotor, although it is also affected by the magnetic field produced by the stator current. In an interior PMSM, the magnetic saturation saliency is usually not significant compared to the structural saliency, and hence it is difficult to use the saturation saliency for rotor position detection. However, in a surface mounted PMSM, the saturation saliency may have to be used because the structure saliency is not significant due to the large equivalent airgap length.

In this paper, a non-linear PMSM model which incorporates both the structural and saturation saliencies is derived. In this model, the saliencies of the motor are reflected by the variation of the stator winding inductances with respect to the rotor positions. In order to obtain the relationship between the inductance and rotor position, an inductance pattern is established based on the experimental measurement of a surface mounted PMSM (SPMSM) and Fourier series. Dynamic performance simulation using the derived model is carried out and the results are compared with those based on the model without considering the saliencies.

II. Non-Linear Model of a PMSM

Fig. 1 illustrates schematically the structure and flux linkage of a SPMSM. When the motor saliencies are taken into account, the conventional model of PMSM is inaccurate since the inductances of the motor are no longer constants and will be the functions of the rotor position and stator current due to the saliencies. Therefore, a new PMSM model is required.

A. Flux Linkage of PMSM

In a PMSM, the rotor field is the dominant field which determines the operating point. Although the characteristic of the magnetic core is non-linear, the magnetic circuit can be considered as piecewisely linearized around the operating point P at a given rotor position, as shown in Fig. 2. Thus, the total flux linkage of phase a, λ_a, can be separated into two components,

$$\lambda_a(i_a,i_b,i_c,i_f,\theta)=\lambda_{as}(i_a,i_b,i_c,i_f,\theta)+\lambda_{af}(i_f,\theta) \qquad (1)$$

where θ is the rotor position, i_a, i_b, and i_c are the stator currents of phase a, b, and c, respectively, i_f is the equivalent magnetization current of PMs on the rotor, λ_{af} the flux linkage component of phase a produced by the PMs, λ_{as} the flux linkage component of phase a corresponding to the resultant stator magnetization current i_{ms}, and the subscript p indicates the peak value.

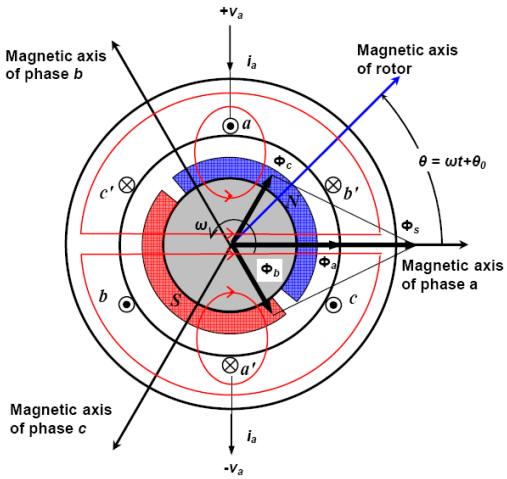

Fig. 1. Structure and flux linkage of an SPMSM.

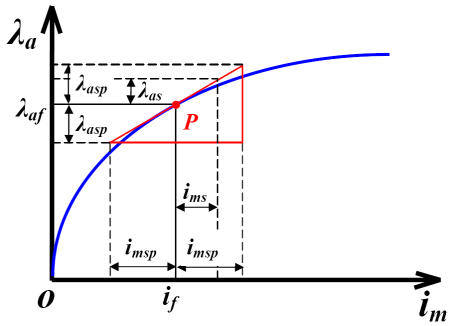

Fig. 2. Linearization of the magnetic circuit in a PMSM.

The flux linkage λ_{as} can be further separated into components attributed to individual stator phase currents

$$\lambda_{as}(i_a,i_b,i_c,i_f,\theta)=\lambda_{aa}(i_a,i_f,\theta)+\lambda_{ab}(i_b,i_f,\theta)+\lambda_{ac}(i_c,i_f,\theta) \tag{2}$$

where λ_{aa}, λ_{ab}, and λ_{ac} are the flux linkage components of phase a generated by the currents in phases a, b, and c, respectively. Consequently, the total flux linkage of phase a is

$$\lambda_a=\lambda_{aa}+\lambda_{ab}+\lambda_{ac}+\lambda_{af} \tag{3}$$

In order to improve the accuracy of the model, the nonlinear saturation effect caused by the stator flux, within every linearization segment of the magnetic circuit, is additionally included even though the assumption of piecewise linearization is applied. The flux linkage components, λ_{aa}, λ_{ab}, and λ_{ac}, can be considered proportional to their corresponding currents

$$\begin{aligned}\lambda_{aa}(i_a,i_f,\theta)&=L_{aa}(i_a,i_f,\theta)i_a\\ \lambda_{ab}(i_b,i_f,\theta)&=L_{ab}(i_b,i_f,\theta)i_b\\ \lambda_{ac}(i_c,i_f,\theta)&=L_{ac}(i_c,i_f,\theta)i_c\end{aligned} \tag{4}$$

The proportionality coefficients L_{aa}, L_{ab}, L_{ac}, which are determined by the slope of the magnetization curve at the operating point, are known as the self- and mutual inductances of the phase windings.

Similarly, the flux linkages of phase b and c are

$$\lambda_b=\lambda_{bb}+\lambda_{ba}+\lambda_{bc}+\lambda_{bf} \tag{5}$$

$$\lambda_c=\lambda_{cc}+\lambda_{ca}+\lambda_{cb}+\lambda_{cf} \tag{6}$$

and then the corresponding self- and mutual inductances, L_{bb}, L_{ba}, L_{bc}, L_{cc}, L_{ca} and L_{cb} are defined.

B. Circuit Equations

If the core losses are neglected, the circuit equations of the three-phase stator windings can be written as

$$v_a=R_a i_a+\frac{d\lambda_a}{dt} \tag{7}$$

$$v_b=R_b i_b+\frac{d\lambda_b}{dt} \tag{8}$$

$$v_c=R_c i_c+\frac{d\lambda_c}{dt} \tag{9}$$

where v_a, v_b and v_c are the phase voltages, R_a, R_b and R_c the phase winding resistances.

Based on the previous derivation, the following differential equations can be obtained

$$\begin{bmatrix}v_a\\v_b\\v_c\end{bmatrix}=\begin{bmatrix}R_a&0&0\\0&R_b&0\\0&0&R_c\end{bmatrix}\begin{bmatrix}i_a\\i_b\\i_c\end{bmatrix}+[L_T]\begin{bmatrix}\frac{di_a}{dt}\\\frac{di_b}{dt}\\\frac{di_c}{dt}\end{bmatrix}+\begin{bmatrix}e_{af}+e_{a\theta}\\e_{bf}+e_{b\theta}\\e_{cf}+e_{c\theta}\end{bmatrix} \tag{10}$$

where

$$[L_T]=\begin{bmatrix}L_{aa}+i_a\frac{\partial L_{aa}}{\partial i_a}&L_{ab}+i_b\frac{\partial L_{ab}}{\partial i_b}&L_{ac}+i_c\frac{\partial L_{ac}}{\partial i_c}\\L_{ba}+i_a\frac{\partial L_{ba}}{\partial i_a}&L_{bb}+i_b\frac{\partial L_{bb}}{\partial i_b}&L_{bc}+i_c\frac{\partial L_{bc}}{\partial i_c}\\L_{ca}+i_a\frac{\partial L_{ca}}{\partial i_a}&L_{cb}+i_b\frac{\partial L_{cb}}{\partial i_b}&L_{cc}+i_c\frac{\partial L_{cc}}{\partial i_c}\end{bmatrix}$$

and $e_{af}=\omega_r d\lambda_{af}/d\theta$, $e_{bf}=\omega_r d\lambda_{bf}/d\theta$, $e_{cf}=\omega_r d\lambda_{cf}/d\theta$ are the electromotive forces (*emf*) induced by the rotor field. The *emf* can be expressed as:

$$e_{a\theta}=\omega_r\left(i_a\frac{dL_{aa}}{d\theta}+i_b\frac{dL_{ab}}{d\theta}+i_c\frac{dL_{ac}}{d\theta}\right) \tag{11}$$

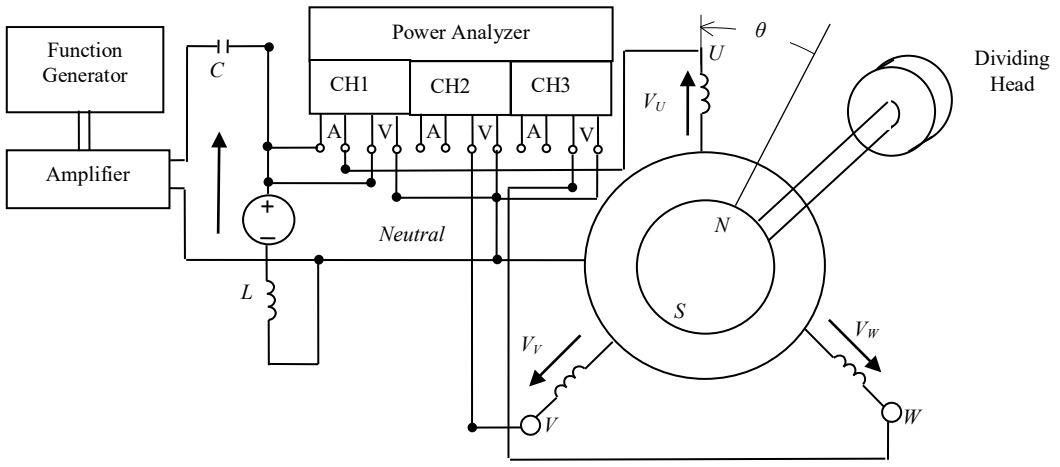

Fig. 3. Setup of the test system.

$$e_{b\theta} = \omega_r \left(i_a \frac{dL_{ba}}{d\theta} + i_b \frac{dL_{bb}}{d\theta} + i_c \frac{dL_{bc}}{d\theta} \right) \quad (12)$$

$$e_{c\theta} = \omega_r \left(i_a \frac{dL_{ca}}{d\theta} + i_b \frac{dL_{cb}}{d\theta} + i_c \frac{dL_{cc}}{d\theta} \right) \quad (13)$$

where $e_{a\theta}$, $e_{b\theta}$ and $e_{c\theta}$ are the *emfs* induced by the variation of flux linkage due to the saliencies, and $\omega_r = d\theta/dt$ is the angular speed of the rotor.

C. Electromagnetic Torque

The electromagnetic torque of the PMSM can be obtained by the derivative of the system co-energy with respect to the rotor angle, $T = \partial W_f'/\partial\theta$. If saturation effect is considered by the linearization method, the co-energy generated by the three phase currents can be found and simplified as: $W_f' = W_a' + W_b' + W_c'$, where

$$\begin{aligned} W_a' &= \int_0^{i_a} \lambda_a(i_a, i_b, i_c, i_f, \theta) di_a \\ &= \frac{L_{aa}(i_f,\theta)}{2} i_a^2 + L_{ab}(i_f,\theta) i_b i_a + L_{ac}(i_f,\theta) i_c i_a \\ &\quad + \lambda_{af}(i_f,\theta) i_a \end{aligned} \quad (14)$$

$$\begin{aligned} W_b' &= \int_0^{i_b} \lambda_b(i_a, i_b, i_c, i_f, \theta) di_b \\ &= L_{ab}(i_f,\theta) i_a i_b + \frac{L_{bb}(i_f,\theta)}{2} i_b^2 + L_{bc}(i_f,\theta) i_c i_b \\ &\quad + \lambda_{bf}(i_f,\theta) i_b \end{aligned} \quad (15)$$

$$\begin{aligned} W_c' &= \int_0^{i_c} \lambda_c(i_a, i_b, i_c, i_f, \theta) di_c \\ &= L_{ac}(i_f,\theta) i_a i_c + L_{cb}(i_f,\theta) i_b i_c + \frac{L_{cc}(i_f,\theta)}{2} i_c^2 \\ &\quad + \lambda_{cf}(i_f,\theta) i_c \end{aligned} \quad (16)$$

The electromagnetic torque can be found as

$$\begin{aligned} T &= \frac{\partial W_a'}{\partial\theta} + \frac{\partial W_b'}{\partial\theta} + \frac{\partial W_c'}{\partial\theta} \\ &= \frac{\partial \lambda_{af}}{\partial\theta} i_a + \frac{\partial \lambda_{bf}}{\partial\theta} i_b + \frac{\partial \lambda_{cf}}{\partial\theta} i_c + \frac{\partial L_{aa}}{\partial\theta} \frac{i_a^2}{2} + \frac{\partial L_{bb}}{\partial\theta} \frac{i_b^2}{2} + \frac{\partial L_{cc}}{\partial\theta} \frac{i_c^2}{2} \\ &\quad + \frac{2\partial L_{ab}}{\partial\theta} i_a i_b + \frac{2\partial L_{ac}}{\partial\theta} i_a i_c + \frac{2\partial L_{bc}}{\partial\theta} i_b i_c \end{aligned} \quad (17)$$

It can be concluded that there are two kinds of electromagnetic torque. One is the torque produced by the rotor field, which is determined by rotor flux linkage, and the other is the torque caused by the inductance variation due to the saliencies.

III. Non-Linear Inductance Pattern

Accurate prediction of the motor dynamic performance requires an accurate presentation of the magnetic characteristics given by the variation of phase inductances. As discussed above, the structural and magnetic saturation saliencies can be reflected by the variation of stator winding inductances, including the self- and mutual inductances. Therefore, an accurate PMSM model by considering the saliencies can be established by a good understanding of the relationship between the inductances and the rotor positions at different current conditions.

A. Inductance Pattern

The phase inductance is a periodic function of angular rotor position. The relation between the phase inductance and the rotor position can be expressed by a Fourier series. Generally, the number of terms of the Fourier series is determined as *(n+1)* for the best curve fitting of the obtained phase inductances [3]. Accordingly, the inductances of the PMSM can be expressed as

$$L(\theta) = a_0 + \sum_{m=1}^{n} \left(a_m \cos m\theta + b_m \sin m\theta \right) \quad (18)$$

In addition, due to the non-linear characteristics of the magnetic core, the inductances vary with the stator current. Consequently, different currents will give different sets of coefficient a_0, a_m, and b_m ($m=1, 2, \ldots, n$). In other words, a_0, a_m, and b_m can be expressed by the functions of related current. Therefore, the inductance can be further expressed as

$$L(i,\theta) = a_0(i) + \sum_{m=1}^{n} \left(a_m(i) \cos m\theta + b_m(i) \sin m\theta \right) \quad (19)$$

For a group of known values of phase inductance, $L(\theta_j, i_k)$, j and k refer to the various rotor position and currents respectively, which can be obtained by either magnetic field analysis or experimental measurement, the inductance pattern can be worked out through the method of non-linear curve fitting.

B. Incorporation of Nonlinear Inductances In PMSM Model With Saliencies

The nonlinear model of the self- and mutual- inductances discussed previously can readily be incorporated into the PMSM model presented in Section 2 by simply substituting the following relationships into the model

$$\frac{dL(\theta, i_k)}{d\theta} = \sum_{m=1}^{n} \left((-m) a_m(i_k) \sin m\theta + m b_m(i_k) \cos m\theta \right) \quad (20)$$

$$\frac{dL(\theta_j, i)}{di} = \frac{da_0(i)}{di} + \sum_{m=1}^{n} \left(\frac{da_m(i)}{di} \cos m\theta_j + \frac{db_m(i)}{di} \sin m\theta_j \right) \quad (21)$$

IV. Measurement of Inductance of PMSM

In order to identify the coefficient matrix used in the modeling, experiments are carried out on a 6-pole SPMSM to measure the self- and mutual inductances at various rotor positions and stator currents.

The system for the measurement is shown in Fig. 3. The rotor of the motor is locked by a dividing head**.** The phase windings are excited by applying a current to one phase while the other two are open. The voltage, current and power of the excited phases are measured and the open-

circuit voltages of the other two phases are also recorded. Based on the circuit analysis of Fig. 3, the self and mutual inductances at different rotor positions and stator currents can be obtained.

The self-inductances of the phase windings at various rotor positions, measured with a stator current of 0.3 A, are illustrated in Fig. 4. It can be seen that there are very little differences between the self-inductances of three phases. The measured mutual inductances are shown in Fig. 5. The inductance model can be applied in the derived non-linear PMSM model.

Based on the nonlinear property of the self and mutual inductances mentioned in Section 3, the following Fourier series are used to express the self and mutual inductances at a given current:

$$L_s(\theta) = a_0 + \sum_{i=1}^{8}\left(a_n \cos n\theta + b_n \sin n\theta\right) \tag{22}$$

$$L_m(\theta) = a_0 + \sum_{i=1}^{8}\left(a_n \cos n\theta + b_n \sin n\theta\right) \tag{23}$$

where the number of terms is chosen as 8. Based on the experimental data, the coefficients of the models of self and mutual inductances can be obtained.

In order to identify the saturation saliency of the stator flux, DC currents are used to make the total magnetic field more saturated at some positions and less saturated at other positions, and the phase inductances are measured with various DC current offsets, which will be discussed later.

It is shown that the inductance variation due to the PMs on the rotor can be identified. With the measured inductances, dynamic simulation is carried out.

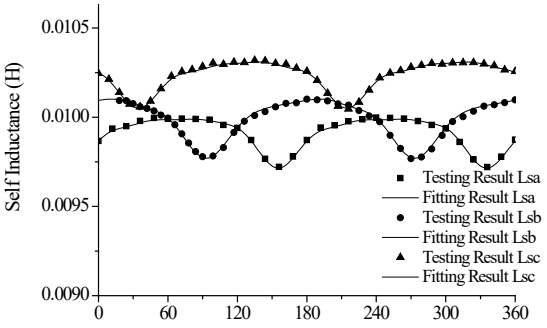

Fig. 4. Measured self-inductances and fitting curves.

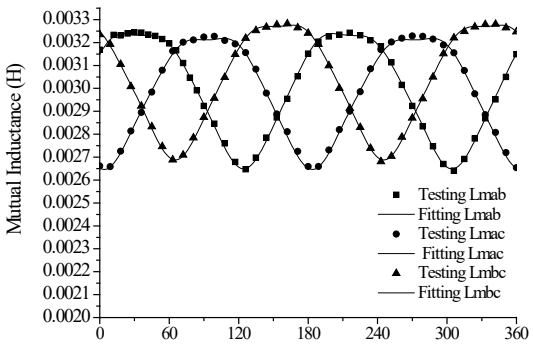

Fig. 5. Measured mutual inductances and fitting curves.

V. Simulation of the Dynamic Performance of the PMSM

A. Parameter Measurement

Based on the model and experimental parameter identification, dynamic simulation of the PMSM using the model incorporating the structural saliency is conducted. The simulation based on the model without considering saliencies is also conducted for comparison.

In order to simulate the performance of the SPMSM, some electrical and magnetic parameters, such as the magnetizing flux linkage (flux linkage produced by permanent magnet), stator winding resistance and inductances are required. Experiments are firstly conducted to measure these parameters.

The magnetizing flux linkage λ_m is obtained by measuring the phase voltage by the open circuit test. The experimental result is: λ_m = 0.118 *Wb*. The stator winding resistances at various temperatures are measured by the VA method in a temperature controllable chamber. The relationship of the phase resistances and motor temperature is obtained as: $R_U=1.579*(1+0.004033T)$, $R_V=1.584*(1+0.004017T)$, and $R_W=1.602*(1+0.003946T)$, where T is the temperature in °C.

B. Simulation Results of the Model by Considering Saliencies

Based on the PMSM model by considering saliencies and the measured parameters, simulation is firstly conducted to estimate the dynamic performance of the motor at no load. The input voltage is a balanced three phase sinusoidal waveform with amplitude of 12 V rms and frequency of 5 Hz.

The stator currents of the motor are shown in Fig. 6. The total back *emf*, and the back *emf* caused by structural saliency are illustrated in Fig. 7 and Fig. 8. The total electromagnetic torque, and the electromagnetic torque caused by structural saliency at no-load are shown in Fig. 9 and Fig. 10. Fig. 11 shows the torques at load.

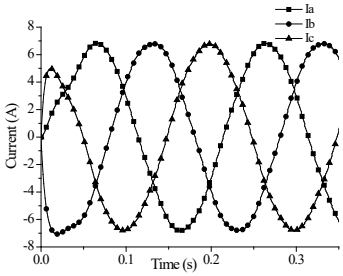

Fig. 6. Phase current by the model with structural saliency.

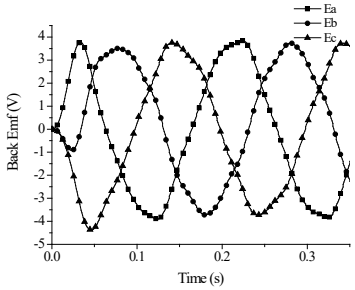

Fig. 7. Total back *emf* by the model with structural saliency.

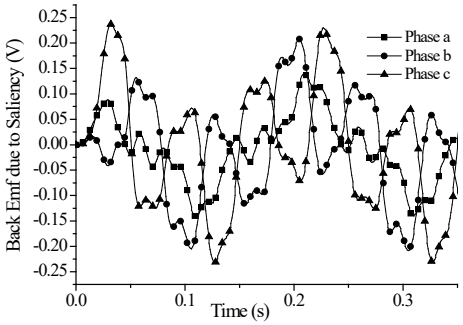

Fig. 8. The back *emf* due to structural saliency.

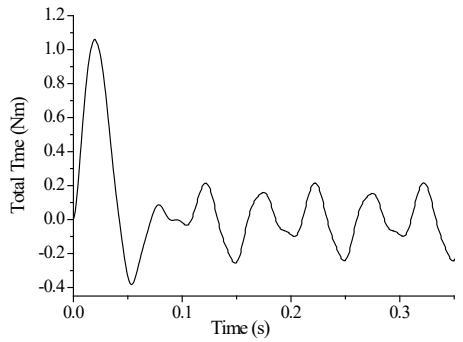

Fig. 9. Electromagnetic torque by the model with structural saliency, at no-load.

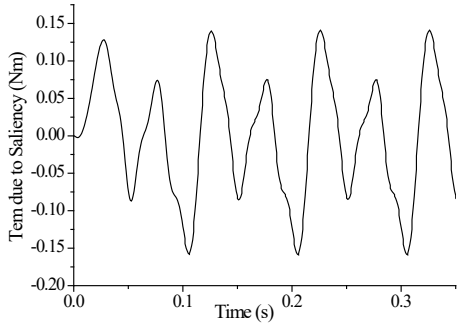

Fig. 10. Electromagnetic torque due to structural saliency, at no-load.

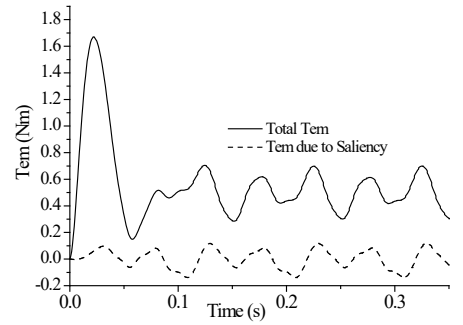

Fig. 11. Total electromagnetic torque and electromagnetic torque caused by structural saliency, with a load of 0.5 Nm.

Form the data in Fig. 7 and Fig. 8, in the steady state, the back *emf* caused by structural saliency is only about 4% of the total back *emf*. It is shown that the total back *emf* of the motor is almost not affected by the back *emf* caused by the structural saliency, which adds some high order harmonic components to the total back *emf*, and this distortion can be neglected.

It can be seen from Fig. 9 and Fig. 10 that a big torque variation is produced due to the structural saliency when the load torque is very small.

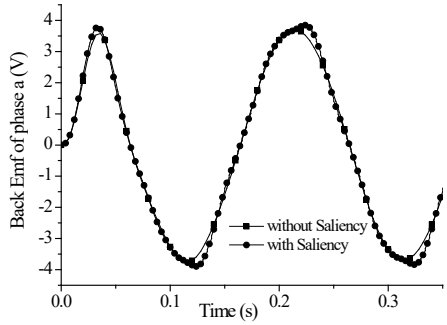

Fig. 12. Comparison of the back *emfs* by the two models.

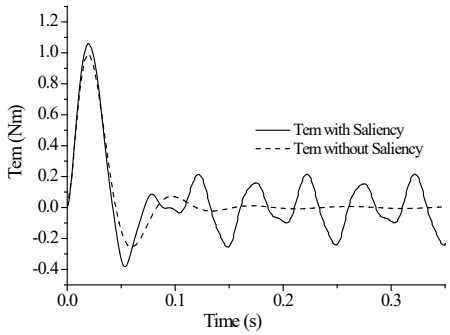

Fig. 13. Comparison of the electromagnetic torque by the two models.

C. Simulation Results of the Model without Considering Saliencies

With the previously measured PMSM parameters, the dynamic simulation for a conventional model without considering saliencies is performed and a Matlab program is complied by using Euler method for the numerical calculation. In order to compare with the previous results, the same initial and load conditions are set in the simulation. The back *emf* and electromagnetic torque are compared with those based on the proposed model with saliency, as shown in Fig. 12 to Fig. 13.

It can be seen from Fig.12 and Fig.13 that very small difference of the back *emf* and electromagnetic torque obtained in those two models is mainly due to the surface-mounted permanent magnet rotor structure. For this specific motor, the saliency effect is not so apparent as motors with large saliencies, such as interior type PMSM or switch reluctance motor. However, the proposed model is capable of analysing various types of motor by considering saliencies. Moreover, the dynamic performance of the motor can be described more accurately with the proposed model. More accurate torque calculation can be useful for the dynamic state estimation in the torque control scheme, such as the direct torque control scheme.

VI. Discussion of the Saturation Saliency

In order to study the saturation saliency of the stator flux, the phase inductances are measured with various DC current offsets applied to the phase windings. With a DC current of 6A applied to phase *a*, the self-inductances of phase *a*, *b* and *c* are measured by the AC voltage-current method and compared with those obtained without DC cur-

rent offset. The results are shown in Fig. 14, Fig. 15 and Fig. 16.

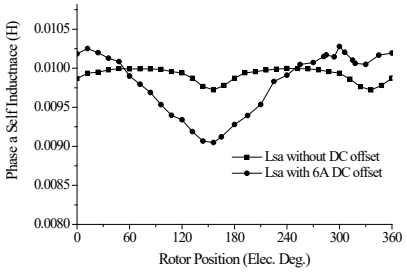

Fig. 14. Inductances of phase *a*, with and without DC offset in phase *a*.

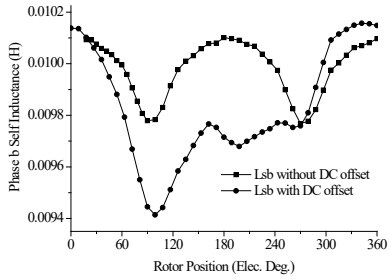

Fig. 15. Inductances of phase *b*, with and without DC offset in phase *a*.

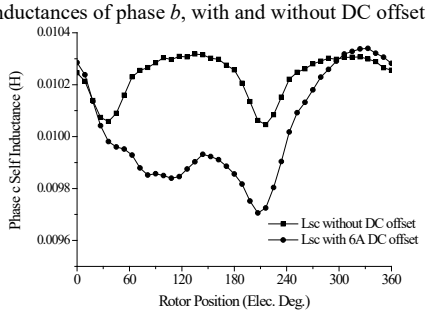

Fig. 16. Inductances of phase *c*, with and without DC offset in phase *a*.

For the inductances without DC currents, due to structural saliency, the magnetic circuit becomes a bit more or less saturated when the axis of the stator windings aligns with that of the rotor flux. As a result, the maximum or minimum values of the inductances appear at those positions. The rotor position could be estimated by identifying the crest or trough values of the inductances, which may correspond to the q- and d-axes of the rotor, although the estimation is difficult due to the small variation. In addition, the inductance variation frequency is twice the main frequency because the variation of inductance is independent of the direction of flux. The rotor pole polarity cannot be directly obtained based on the map of the inductances.

For the experimental results of the inductances with DC offset shown in Figs. 14-16, the axis of the stator flux aligns with that of the phase *a* winding. At the positions where the stator flux is perpendicular to the rotor flux, the stator flux has no much effect on the inductance values. Therefore, the inductances obtained with DC offset and without DC offset are close to each other at these locations.

At the positions where the rotor flux aligns with the stator flux, the magnetic filed is more saturated than that at other positions. Therefore, the inductance variation at that position should be large, especially in phase *a*. In Fig. 14, the maximum variation value occurs at about 145º electrical, where the rotor flux aligns with the axis of phase *a*. Meanwhile, for the other two phases, the rotor flux does not align with the axes of the windings and the maximum inductance variations occur close to the axis of phase *a* but different from that of phase *a*.

The inductance variation is mainly caused by the magnetic saturation saliency in this motor. If the variation pattern of the inductances under various rotor positions and stator fluxes could be obtained and mapped, the angle between the rotor flux and stator flux could be estimated, and then the rotor position can be obtained by the known position of stator flux. Based on the analysis, further work could be carried out for sensorless rotor position detection method.

VII. Conclusions

A non-linear PMSM model incorporating both the structural and magnetic saturation saliencies was derived in this paper. In the equivalent electric circuit, the saliencies are reflected by the variation of the stator winding inductances with respect to the rotor positions and stator currents. The nonlinear inductances at various rotor positions are discussed and experimentally obtained from a surface mounted PMSM. Fourier series analysis is employed to describe the relation of the inductance and rotor position based on the experimental results. Dynamic simulation considering the structural saliency is performed based on the parameters obtained from the testing motor. The results are compared with that from a model without considering saliency. It is found that, due to the surface mounted structure of the testing motor, there are only very small differences between the results with and without structural saliencies.

The saliency in the studied SPMSM is mainly due to the magnetic saturation and could be used to estimate the angle between rotor flux and stator flux, which can provide a possibility of initial rotor position estimation for the sensorless PMSM drives. The proposed model is capable of analysing various types of motor by considering saliencies.

References

[1] P.L. Jansen, and R.D. Lorenz, “Transducerless position and velocity estimation in induction and salient AC machines,” in *Record of IEEE IAS Annual Meeting*, Oct. 1994, vol. 1, pp. 488-495.

[2] L. Wang and R.D. Lorenz, “Rotor position estimation for permanent magnet synchronous motor using saliency-tracking self-sensing method,” in *Record of IEEE IAS Annual Meeting*, Oct. 2000, vol. 1, pp. 445–450.

[3] P. Cui, J.G. Zhu, Q.P. Ha, G.P. Hunter and V.S. Ramsden, “Simulation of non-linear switched reluctance motor drive with PSIM,” in *Proc. 5th Int. Conf. on Electrical Machines and Systems*, Aug. 2001, vol. 1, pp. 1061-1064.